Published online 05 May 2009

Nucleic Acids Research, 2009, Vol. 37, No. 12 ***4043–4054***
doi:10.1093/nar/gkp297

Structural and dynamic characterization of the upper part of the HIV-1 cTAR DNA hairpin

Loussiné Zargarian, Igor Kanevsky, Ali Bazzi, Jonathan Boynard, Françoise Chaminade, Philippe Fossé and Olivier Mauffret*

Laboratoire de Biotechnologies et Pharmacologie génétique Appliquée (LBPA), UMR 8113 CNRS, Ecole Normale Supérieure de Cachan, 61 Avenue du Président Wilson, 94235 Cachan cedex, France

Received September 23, 2008; Revised March 17, 2009; Accepted April 15, 2009

ABSTRACT

First strand transfer is essential for HIV-1 reverse transcription. During this step, the TAR RNA hairpin anneals to the cTAR DNA hairpin; this annealing reaction is promoted by the nucleocapsid protein and involves an initial loop–loop interaction between the apical loops of TAR and cTAR. Using NMR and probing methods, we investigated the structural and dynamic properties of the top half of the cTAR DNA (mini-cTAR). We show that the upper stem located between the apical and the internal loops is stable, but that the lower stem of mini-cTAR is unstable. The residues of the internal loop undergo slow motions at the NMR time-scale that are consistent with conformational exchange phenomena. In contrast, residues of the apical loop undergo fast motions. The lower stem is destabilized by the slow interconversion processes in the internal loop, and thus the internal loop is responsible for asymmetric destabilization of mini-cTAR. These findings are consistent with the functions of cTAR in first strand transfer: its apical loop is suitably exposed to interact with the apical loop of TAR RNA and its lower stem is significantly destabilized to facilitate the subsequent action of the nucleocapsid protein which promotes the annealing reaction.

INTRODUCTION

The reverse transcription of the HIV-1 genome consists of a complex succession of events leading to the synthesis of a double-stranded DNA from a single-stranded genomic RNA (1,2). An essential step of this process is the first strand transfer that requires the repeat (R) sequences at both ends of the genome. During this reaction, the minus-strand strong-stop DNA (ss-cDNA), the first product of reverse transcription, is transferred to the 3′-end of the viral RNA in a reaction mediated by base pairing of the complementary R sequences at the 3′-ends of the RNA and DNA molecules. The R RNA sequence can fold into secondary structures corresponding to the transactivator response element (TAR) hairpin (Figure 1) and the upper part of the poly(A) hairpin (3). Similarly, the R sequence of ss-cDNA is predicted to fold into hairpins that are complementary to the TAR and poly(A) RNA sequences and are therefore named cTAR (Figure 1) and cpoly(A), respectively. *In vitro* studies suggest that the TAR structure is far more important than the poly(A) hairpin in minus-strand transfer (4–7).

The HIV-1 nucleocapsid protein (NC) is a nucleic acid binding protein that possesses nucleic acid chaperone activity (2). This chaperone function is due to two independent activities: aggregation of nucleic acids and destabilization of nucleic acid duplexes (2). NC plays a crucial role in minus-strand transfer by facilitating annealing of the complementary R sequences (2). Unfolding of the TAR and cTAR hairpins is thought to be rate-limiting in the annealing process (2,8). Godet *et al.* (9) reported that cTAR DNA-TAR RNA annealing depends on nucleation through the 3′/5′ termini, resulting in the formation of a 'zipper' intermediate. This is in contrast to the results of studies suggesting nucleation through the hairpin loops forming a 'kissing' complex (5,6). Single-molecule FRET studies support the notion that there may be multiple pathways for the annealing of cTAR DNA to TAR RNA (10–12). Whatever the mechanism, the complex develops to become an extended duplex in which the two partners are totally annealed.

Thermodynamic data suggest that the top half of the cTAR hairpin is more stable than the bottom half (13,14). Using single-molecule spectroscopy (SMS) techniques, Liu *et al.* (11) showed that the cTAR hairpin reactant is predominantly a single NC-coated hairpin with a dynamic secondary structure, involving equilibrium between a 'Y' shaped and a closed conformation. In the 'Y' conformation, the lower stems are open and the upper stems are closed. The annealing process has been investigated using the mini-TAR and mini-cTAR sequences to assess the roles of the top halves of TAR and cTAR

*To whom correspondence should be addressed. Tel: +33 1 47 40 77 33; Fax: +33 1 47 40 76 71; Email: olivier.mauffret@lbpa.ens-cachan.fr

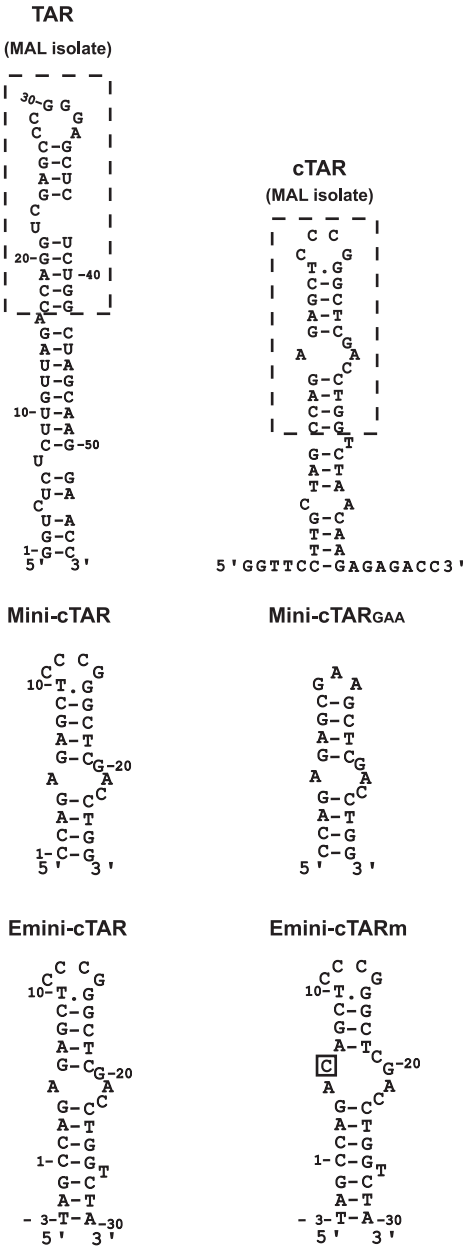

Figure 1. Predicted secondary structures for the TAR and cTAR sequences. Zuker's (42) folding programs were used to predict the most stable secondary structures for RNA and DNAs. The top parts of TAR and cTAR hairpins are indicated by the dotted boxes. The mini-cTAR sequence is derived from the top part of the cTAR hairpin. Numbering of extended mini-cTAR (Emini-cTAR) is relative to mini-cTAR. The single base mutation at position 6 is boxed in the Emini-cTARm sequence.

hairpins (14,15) (Figure 1). NC-induced destabilization of mini-cTAR depends on the internal loop: this loop is a melting initiation site and probably a binding site for NC (14). The way in which the internal loop destabilizes mini-cTAR is unknown. The apical loop of mini-cTAR does not seem to be significantly involved in NC-mediated melting, although it is probably a binding site for NC (14). The stem ends and the apical loops of mini-TAR and mini-cTAR are the sites for initiation of the annealing reaction, i.e. the 'zipper' and 'kissing' intermediates are probably involved in the annealing process (15).

Structural and dynamic studies for completing the thermodynamic and kinetic data would greatly help elucidate the role of the apical stem-loops in the first strand transfer (14,15). The mini-TAR RNA structure has been extensively studied using NMR and X-ray methods (16–19). In contrast, mini-cTAR DNA has not been studied using these methods. Here, the structural and dynamic properties of mini-cTAR were characterized using NMR and probing methods. The mini-cTAR molecule investigated in this study is identical to the (14–39) cTAR molecule previously studied by fluorescence methods (14). To resolve the assignment difficulties, we also investigated a derived sequence in which the apical loop has been replaced by the GAA loop whose the NMR signature is well known (20). To identify the structural and dynamic properties of mini-cTAR, we conducted combined NMR studies of the original and derived sequences. We showed that the apical loop of mini-cTAR is poorly organized and its internal loop is a conformational exchange site which strongly destabilizes the lower stem but not the upper stem. It is likely that this asymmetric destabilization is important for NC-mediated annealing of cTAR DNA to TAR RNA.

MATERIALS AND METHODS

Samples preparation

Unlabeled mini-cTAR DNA (26 nt) was obtained from Eurogentec; and $^{15}N/^{13}C$ labeled mini-cTAR DNA (also 26 nt) was obtained from SILANTES. For NMR studies, the unlabeled and labeled mini-cTARs were dissolved in 450 µl and 300 µl (shigemi tube), respectively, of 10 mM phosphate sodium buffer (pH 6.5), 30 mM NaCl, 0.2 mM $MgCl_2$. The final concentrations of the unlabeled and labeled species were 1.5 mM and 0.75 mM, respectively.

Enzymatic and $KMnO_4$ probing of mini-cTAR

Potassium permanganate and piperidine were purchased from Sigma-Aldrich. Mung bean nuclease, S1 nuclease and DNase I, were purchased from New England Biolabs, Roche Molecular Biochemicals and Promega, respectively. The renaturation buffers contained: 125 mM Tris–HCl (pH 7.5), 150 mM NaCl, 1 mM $MgCl_2$ for probing with $KMnO_4$ or DNase I; 250 mM NaOAc (pH 5.0), 150 mM NaCl, 5 mM $ZnSO_4$, 1 mM $MgCl_2$ for probing with mung bean nuclease; and 250 mM NaOAc (pH 5.0), 1.4 M NaCl, 5 mM $ZnSO_4$, 1 mM $MgCl_2$ for probing with S1 nuclease. Mini-cTAR DNA was 5′-end labeled using T4 polynucleotide kinase (New England Biolabs) and [γ-^{32}P] ATP (Perkin Elmer). The 5′-end-labeled mini-cTAR was purified by electrophoresis on a 15% denaturing polyacrylamide gel and isolated by elution followed by ethanol precipitation. Probing assays were carried out in a final volume of 10 µl. Labeled mini-cTAR (100 pmol at 3×10^2 cpm/pmol) in 8 µl of water, was heated at 90°C for 2 min and chilled for 2 min on ice. Then, 2 µl of renaturation buffer was added

and the sample was incubated for 30 min at 20°C. At the end of this incubation, samples were incubated with $KMnO_4$ or an enzyme as follows: 0.5 or 2 U of mung bean nuclease for 17 min at 20°C; 0.1, 0.2 or 0.4 U of S1 nuclease for 12 min at 20°C; or 0.05, 0.1 or 0.2 U of DNase I for 10 min at 20°C. These cleavage reactions were stopped by phenol–chloroform extraction followed by ethanol precipitation. The dried pellets were resuspended in 4 µl of loading buffer (7 M urea, 0.03 w/v% bromophenol blue and 0.03 w/v% xylene cyanol).

For potassium permanganate probing, mini-cTAR DNA was treated with 0.5, 1 or 2 mM of $KMnO_4$ for 1 min at 20°C. The treatment was stopped by adding 40 µl of the termination buffer (0.7 M β-mercaptoethanol, 0.4 M NaOAc (pH 7.0), 10 mM EDTA, 25 µg/ml tRNA). Mini-cTAR was then extracted with phenol–chloroform, ethanol precipitated and dried. Mini-cTAR was subjected to piperidine cleavage by resuspension of the dried pellet in 100 µl of freshly diluted 1 M piperidine and heating at 90°C for 30 min. The samples were then lyophilized, resuspended in 20 µl of water, and lyophilized again. After a second lyophilization from 15 µl of water, the samples were resuspended in 4 µl of loading buffer. G and T + C sequence markers of the labeled mini-cTAR were produced by the Maxam-Gilbert method (21). All samples were analyzed on denaturing 17% polyacrylamide gels.

NMR spectroscopy

All NMR spectra were acquired on Bruker Avance 500 MHz spectrometer. Nonexchangeable protons resonances were assigned in D_2O using 2D NOESY, TOCSY COSY spectra. Additional experiments were performed using the $^{15}N/^{13}C$ sample: constant time HSQC ^{1}H-^{13}C, 3D NOESY-HSQC [^{1}H,^{13}C,^{1}H] (acquired separately with optimization for aromatic and ribose correlations) to assign 1H and aromatic and 1′ carbons. In the ^{1}H-^{13}C HSQC experiments the cross-peaks intensities were measured from peak heights. The NOESY spectra were recorded with mixing times of 50, 80, 120, 200 and 300 ms. Exchangeable protons were assigned using 2D NOESY spectra recorded in 90/10% H_2O/D_2O mixture at 10, 20 and 30°C. ^{1}H-^{31}P HETCOR experiments were run at 20°C.

Structural restraints

Bounds for interproton distances were estimated from NOESY spectra recorded at several mixing times. The distances restraints were classified into categories on the basis of NOE intensities observed: strong NOEs (1.8–3 Å), medium NOEs (1.8–4.5 Å), weak NOEs (3.0–6.0 Å) and very weak NOEs (4.0–7.0 Å). The restraints for torsion angles, hydrogen bonds and planarity was applied using standard methods as described in Renisio *et al.* (22).

Structure calculations

The structure of mini-cTAR was calculated using torsion angle molecular dynamics (TAMD) and the XPLORNIH program (23,24). The methodology is similar to that described by Renisio *et al.* (22). Fifty starting structures with randomized torsion angles were submitted to a simulated annealing restrained molecular dynamics protocol in torsion angle space, followed by Cartesian molecular dynamics. The six best-energy structures were selected, analyzed and visualized using the PYMOL program.

RESULTS

Analysis of mini-cTAR secondary structure

Mini-cTAR at a concentration of 20 µM was in a monomer conformation and did not form duplexes as assessed by native gel electrophoresis (data not shown). Mini-cTAR DNA was probed with potassium permanganate ($KMnO_4$), mung bean (MB) nuclease, S1 nuclease and DNase 1 (Figure 2). MB and S1 nucleases are highly selective for single-stranded nucleic acids and single-stranded regions in double-stranded nucleic acids (25). DNase I is a double-strand-specific endonuclease that produces single-strand nicks (26). $KMnO_4$ can be used to detect regions of DNA that are unpaired or distorted (27,28): it is an oxidizing agent that preferentially attacks the 5,6 double bond of thymine. In B-DNA, this bond is shielded by base stacking interactions and, thus, the T residues in such DNA duplexes are relatively resistant to oxidation. After treatment of mini-cTAR DNA with piperidine, the DNA backbone was cleaved at the site of the modified thymines. The cleavage fragments generated by the nucleases and the $KMnO_4$/piperidine treatment were analyzed by electrophoresis on denaturing 17% polyacrylamide gels (Figure 2). The cleavage sites were identified by running Maxam-Gilbert sequence markers of mini-cTAR on the same gels in parallel. Note that the nucleases cleave the phosphodiester bond and generate a 3′-hydroxyl terminus on 5′-end labeled DNA. In contrast, the $KMnO_4$/piperidine treatment and Maxam–Gilbert reactions generate a 3′-phosphorylated terminus on 5′-end labeled DNA (21,29). The electrophoretic mobility of Maxam-Gilbert sequence markers is therefore slightly greater than that of fragments produced by nucleases (Figure 2A, lanes G and T + C): the difference in electrophoretic mobility was less than the distance between two succeeding nucleotides in the case of mini-cTAR.

There were strong and moderate MB and S1 cleavages between C_{12}, C_{13} and C_{13}, G_{14} (Figure 2A), all of which are predicted to lie within the apical loop of mini-cTAR (Figure 2C). The high sensitivity of T_{10} to $KMnO_4$ (Figure 2B) indicates that at least one side of the plane of the heterocyclic ring is exposed. This suggests that the predicted T.G mismatched base-pair is not involved in strong stacking interactions with the residues of the apical loop. Consistent with the formation of the upper stem (Figure 2C), the sensitivity of T_{18} to $KMnO_4$ was very low (Figure 2B). In addition, the site between C_9 and T_{10} was highly sensitive to DNase I cleavage (Figure 2A) providing evidence that the upper stem is formed. Surprisingly, there were strong and moderate MB and S1 cleavages within the sequence between positions 23–26 (Figure 2A) that is predicted to be double-stranded (Figure 2C). In addition, the putative stacking interactions between T_{24} and the flanking G–C base-pairs

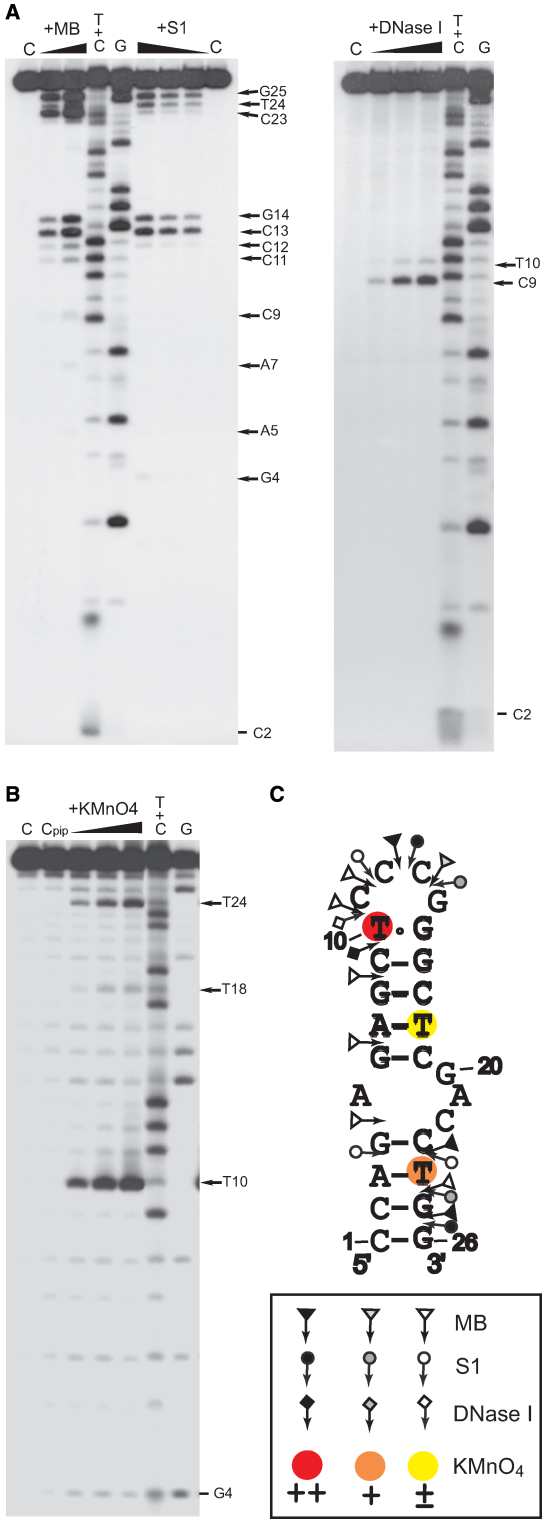

Figure 2. Analysis of mini-cTAR secondary structure. Enzymatic and $KMnO_4$ probing experiments were performed as described in Materials and Methods section. (**A**) The 5′-end-labeled mini-cTAR was incubated with mung bean (MB) nuclease (0.5 and 2 U), S1 nuclease (0.1, 0.2 and 0.4 U) or DNase I (0.05, 0.1 and 0.2 U). Lanes C are controls without enzyme. G and T+C refer to Maxam-Gilbert sequence markers. Arrows indicate the cleavage sites. (**B**) 5′-end-labeled mini-cTAR was incubated with $KMnO_4$ (0.5, 1 and 2 mM). Lane C is the control without any chemical treatment. Lane C_{pip} is the control without $KMnO_4$ treatment but with piperidine treatment. Arrows indicate the reactive thymine residues. (**C**) The most stable mini-cTAR secondary structure predicted by mfold (42). Closed, gray and open symbols indicate strong, medium and weak cleavage sites, respectively, for the various enzymes (triangle for mung bean nuclease, circle for S1 nuclease and diamond for DNase I). The color codes used for the reactivity of thymine residues are indicated in the inset.

are not supported by the sensitivity of T_{24} to $KMnO_4$ (Figure 2B). These various findings indicate that the putative lower stem is not formed or that the base pairing interaction between nucleotides $_1CCAG_4$ and $_{23}CTGG_{26}$ is only transient. To conclude, the probing data exclude the possibility that the lower stem forms a stable double-stranded structure.

NMR assignments

The mini-cTAR$_{GAA}$ (Figure 1) was designed to help in the assignment of the mini-cTAR resonances. The residues of the apical and internal loops of mini-cTAR are expected not to be in B-DNA conformations, making the assignment task much more complicated. In the mini-cTAR$_{GAA}$ molecule, the $_{10}TCCCGG_{15}$ sequence of mini-cTAR has been replaced by the GAA sequence whose the NMR signature is well known (20). Note that the two base-pairs flanking the GAA sequence in mini-cTAR$_{GAA}$ are identical to those in the molecule studied by Hirao *et al.* (20). Analysis of the NOESY spectra of mini-cTAR$_{GAA}$ allowed the assignment of the GAA resonances that appeared at similar positions in our work and in that of Hirao *et al.* (20). Following this assignment, the upper and lower stems of mini-cTAR$_{GAA}$ were identified on the basis of the presence of idiosyncratic NOEs associated with the B-form DNA (data not shown). The four remaining residues, associated with the internal loop were unambiguously assigned, the adenines A_5 and A_{21} being identified by the connectivities that they provide to their neighbor residues. After the assignment of mini-cTAR$_{GAA}$, we reported these assignments in the 2D spectra of mini-cTAR. In addition, the six resonances associated with the $_{10}TCCCGG_{15}$ sequence were assigned. The 3D spectra NOESY HSQC [^{1}H,^{13}C,^{1}H] allowed the difficult cases to be resolved (data not shown).

Surprisingly, we observed only four imino signals at 10°C which appear in the region of resonances associated with Watson–Crick base pairing (Figure 3) although at least eight base-pairs were expected from the predicted secondary structure (Figure 1). The assignment procedure established that the observable imino protons are those of residues G_6, G_8, G_{16} and T_{18}, i.e. the residues of the upper stem. The G_{16} imino proton was the first signal that disappeared as the temperature was increased. The absence of detectable imino proton associated to the apical loop show that this latter is weakly structured and in particular we did not find any evidence of T.G base pairing, despite mfold predictions suggesting that this pairing should occur (Figure 1). The two stems behave very differently: the imino protons of the base-pairs of the upper stem were detected but not those of the lower stem. The nonobservation of imino protons is related to rapid exchange of imino protons with the solvent. This is consistent with the

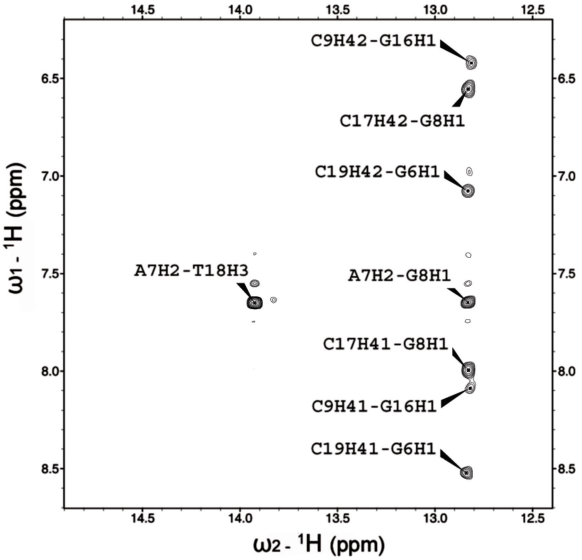

Figure 3. Selected region of 2D NOESY (200 ms mixing time) spectrum of mini-cTAR at 10°C recorded in $^{2}H_2O$. The region is that of the imino to H2/amino connectivities. The main intra and inter base-pair cross-peaks are labeled and the protons involved are indicated.

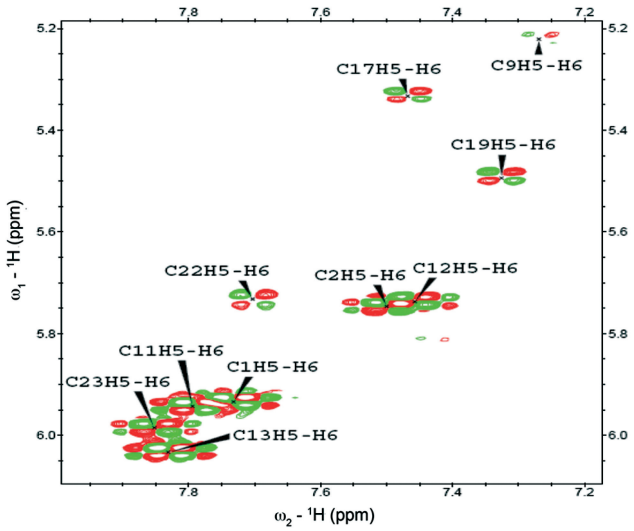

Figure 4. H5–H6 region of 2D COSY spectrum of mini-cTAR at 20°C recorded in $^{2}H_2O$. The H5–H6 cross peaks are labeled with the name of the residue.

probing data indicating that the lower stem does not form a stable double-stranded structure.

Analysis of NOE data

NOE data was visualized using 2D NOESY and 3D NOESY HSQC ^{1}H-^{13}C spectra, the latter being used when the overcrowding of the resonances hampered assignment and estimation of the intensities of NOEs contacts. We used also the 2D spectra obtained with the mini-cTAR$_{GAA}$: the spectra for this molecule are less overcrowded because the base protons of the GAA loop and the base protons of the internal loop resonate in different regions. In the mini-cTAR spectra, the base resonances of residues C_{11}, C_{13}, G_{14} and G_{15} are in the same region as the base protons of residues A_5 and A_{21} making the identification of NOEs more difficult. Sequential H1′(i), H2′/H2″(i), H3′(i) to aromatic (i + 1) are observed for residues C_1 to G_4, C_{23} to G_{26}, G_6 to C_9 and G_{16} to C_{19} indicating that these portions of mini-cTAR adopt a helical B-type geometry for each strand. Therefore, each strand of the lower stem is structured in a B-DNA form despite no imino protons are detected. However, this observation does not demonstrate that the lower stem forms a stable double-stranded B-helix. Analysis of the NOEs for the internal loop and the flanking base pairs clearly showed the presence of numerous sequential NOEs between A_5-G_6, C_{19}-G_{20} and G_{20}-A_{21} steps. In contrast, several sequential NOEs are absent for the A_{21}-C_{22} and C_{22}-C_{23} steps. Residues T_{10}, G_{14} and G_{15} exhibit sequential NOEs to their-neighbors indicating some degree of organization. Residues C_{11}, C_{12} and C_{13} display very few contacts to others residues and are difficult to assign individually.

Linewidth broadening of residues

Large differences in the linewidth of several base and sugar resonances were observed. The molecule was characterized by a variety of behaviors with some residues presenting evidence of exchange broadening whereas others resonances appeared particularly narrow. The H5–H6 region of COSY illustrates these features well: the cross-peaks H5–H6 of residues that are located in the lower stem (C_1, C_2 and C_{23}) and in the apical loop (C_{11}, C_{12} and C_{13}) are much more intense than the cross-peaks of residues C_9, C_{17}, C_{19} and C_{22} (Figure 4). These strong intensities reflect substantial mobility of residues and indicate that the lower stem is dynamic, consistent with the lack of imino signals. In addition, the three cytosines in the apical loop were found to be mobile in agreement with the scarcity of internucleotide NOE data for these residues. In contrast, the residues of the upper stem and the cytosine 22 of the internal loop did not show evidence of high mobilities. In the different 2D spectra, the base resonances of G_4, A_5, A_{21} and C_{22} are broadened in a temperature-sensitive way; this is particularly well illustrated in the 2D spectra for mini-cTAR$_{GAA}$ that are less overcrowded (data not shown).

^{31}P experiments

A 2D ^{1}H-^{31}P spectrum of mini-cTAR was recorded (Figure 5). Using the H3′ resonance assignments, it is possible to assign some phosphorus signals that are well separated from the others. The $C_{13}pG_{14}$ and $C_{12}pC_{13}$ phosphates resonate at high field (−4.5 ppm) from the main group of phosphorus resonances. An extremely low field shifted (−3.1 ppm) signal was assigned to the G_4pA_5 phosphate and revealed a highly distorted backbone conformation in the internal loop. Note that for these high and low-field shifted phosphorus resonances, no ^{31}P-H4′ cross-peaks were detected indicating atypical

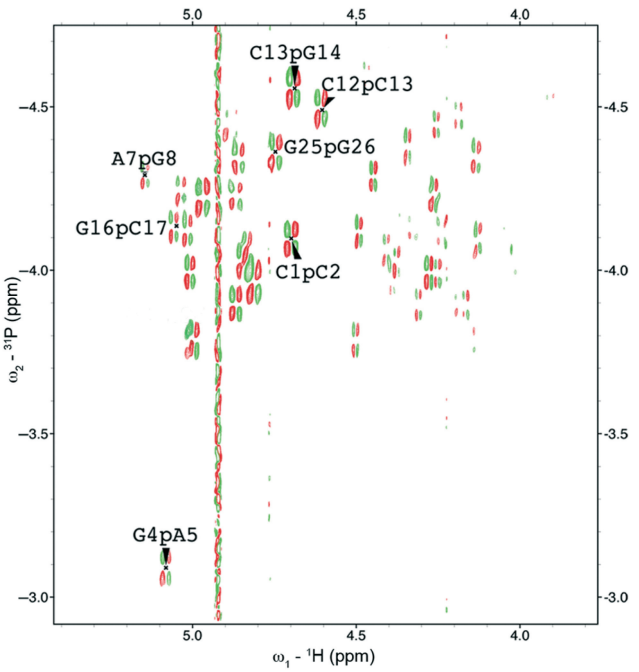

Figure 5. ^{1}H-^{31}P HETcor spectrum of mini-cTAR at 30°C. Some H3′-^{31}P have been assigned and are labeled with the two residues connected to the observed ^{31}P. Note that the G_4pA_5 is highly low-field shifted in the ^{31}P dimension.

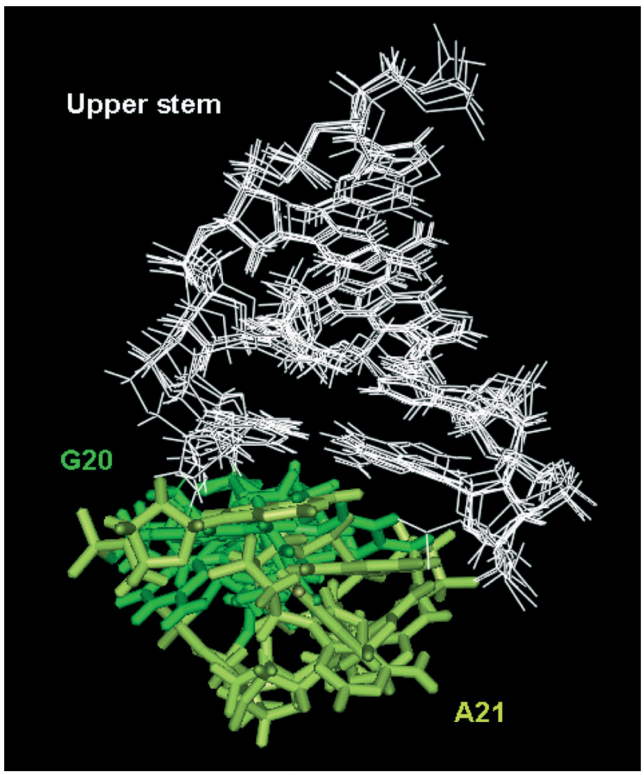

Figure 6. View of the six best-energy conformers of the upper stem and residues G_{20} and A_{21} of the internal loop of mini-cTAR calculated with NMR restraints. The molecules are superimposed on the basis of the upper stem which is colored in white.

backbone conformations. In contrast, ^{31}P-H4′ cross-peaks are present for the resonances of the stem indicating backbone conformations consistent with the B-DNA form.

Structure calculations

The ensemble of the NOE, dihedral angle and hydrogen bond restraints was used for structure calculations. The calculations did not converge on a well-defined family of structures for the apical and internal loops. The global superposition of the structures is rather poor. The residues of the apical loop appear poorly organized compared to those of the upper stem (Supplementary Figure 1). Interestingly, residues T_{10} and G_{15} do not form the T.G mismatched base pair predicted from mfold predictions. However, it appears that residue T_{10} exhibits moderate and weak stacking interactions with residues C_9 and C_{11}, respectively. In the internal loop, residue A_5 is poorly defined being directed towards the interior of the internal loop in some conformers and towards the solvent in others, whereas residues G_{20} and A_{21} are relatively stacked (Figure 6). Residue C_{22} extrudes from the loop in several conformations. Residues G_4 and C_{23} are paired in some but not most conformers. Among the six best conformers, we searched for the stabilizing interactions between residues of the internal loop. Views of three of these conformers indicating the interactions between residues of the internal loop are presented in Figure 7. Residue A_5 was found to interact via hydrogen bonding with G_{20} (Figure 7A) in some conformers and via stacking interactions with residue A_{21} (Figure 7A and C) or residue G_{20} (Figure 7B) in others. Thus, the calculated structures are consistent with alternative conformations in the internal loop. Concerning the lower stem, no well-defined structures emerged from calculations performed without any restraints on base-pairs. However, within the five best-energy conformers (Supplementary Figure 2), the G_4 and C_{23} facing bases and the A_3 and T_{24} facing bases appear to be in near proximity, but the conformers do not exhibit any preferential mode for base pairing. The two strands of the lower stem display a large variety of geometries. However, it appears that the average geometry of the $_{23}CTGG_{26}$ strand is better defined than that of the $_{1}CCAG_4$ strand. Nevertheless, the relative arrangement of the two ends is undetermined, likely due to fraying affecting the outermost residues (Supplementary Figure 2).

^{13}C NMR

2D ^{1}H-^{13}C spectra performed on uniformly labeled $^{15}N/^{13}C$ samples allowed confident assignment of carbon and proton resonances. First, we studied an unlabeled sample but this gave nonassignable spectra. Indeed, several cross-peaks were absent from the 1′ and bases region. The same spectra recorded from the labeled samples showed that the cross-peaks in these regions had very weak intensities due to substantial line broadening. The ^{1}H-^{13}C aromatic correlation cross peaks are highly informative because the different types of residues resonate in specific regions, thus allowing resonances to be definitely assigned (Figure 8A). Also, the ^{1}H-^{13}C spectra revealed

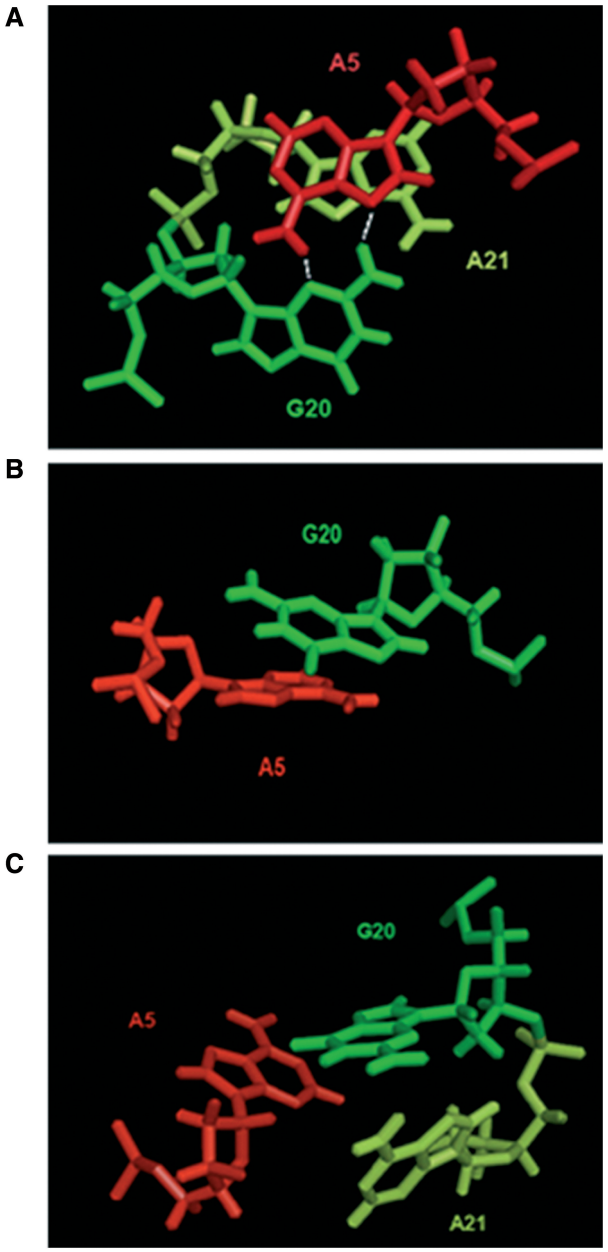

Figure 7. Three views of pairing or stacking interactions of the residues A_5, G_{20} and A_{21} of the internal loop observed in three of the six best-energy conformers of mini-cTAR. (**A**) In this conformer, residues A_5 and G_{20} contact each other through hydrogen bonds (represented as white lines). (**B**) In this conformer, residues A_5 and G_{20} stack each other. (**C**) In this conformer, residues A_5 and G_{20} stack each other and G_{20} stacks with A_{21}. These views show the various interactions that the A_5 residue can undertake with the other residues in the internal loop.

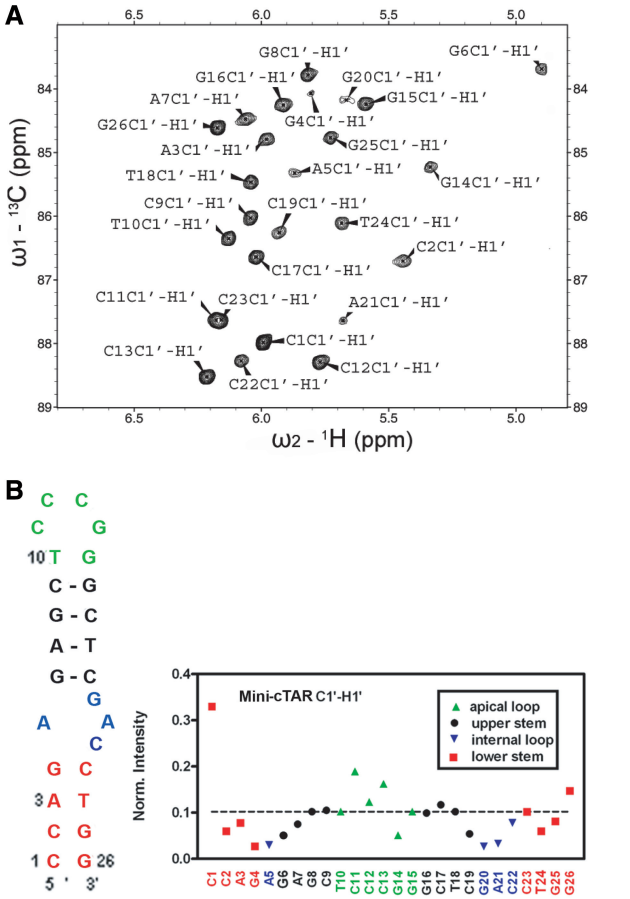

Figure 8. Region H1′–C1′ of constant-time HSQC of $^{15}N/^{13}C$ labeled mini-cTAR at 20°C. (**A**) The cross peak is indicated with the name of the residue. (**B**) Normalized resonance intensities of C1′-H1′ cross-peaks measured from constant time 2D ^{1}H-^{13}C HSQC spectrum of mini-cTAR at 20°C. Red squares for the lower stem, blue triangles for the internal loop, green triangles for the apical loop and black circles the upper stem. The dashed lines correspond to mean values for the upper stem.

that the G_6 H1′ resonance is shifted at high-field and resonates in the H3′ region. This information was almost impossible to deduce from the 2D NOESY and COSY spectra only.

The cross-peaks intensities H1′-C1′ (Figure 8A) can be used as indicators of the motional modes of the various residues. As reference values, we used the mean intensities of the H1′-C1′ cross-peaks of the upper stem which is the most structured part of the molecule (Figure 8B). Relative to these intensities, some cross-peaks present higher intensities indicating fast motions in the picosecond–nanosecond time scale (30,31). Others cross-peaks possess lower intensities indicating exchange broadening in agreement with intermediate/slow exchange processes in the microsecond/millisecond range (30,31). Thus, it appears that the apical loop and the terminal residues (C_1, C_{11}, C_{13} and G_{26}) exhibit fast motions, and the internal loop residues (A_5, G_{20} and A_{21}) and the adjacent G_4 residue display slow conformational exchange (Figure 8B). The presence of local fast motions in the apical loop suggests that it is extremely dynamic and poorly structured. The C1′-H1′ data suggest that the three cytosines of the apical loop are the most dynamic residues other than the two terminal residues. Residues T_{10}, G_{14} and G_{15} are probably involved in transient interactions since they are not so mobile.

The exchange broadening phenomena in the internal loop are clearly established by the ^{13}C NMR data. The broadening is extended to the nearest neighbors of the

lower stem residues and residue G_4 is the most affected. The exchange-broadened residues probably sample more than one conformation. This is in agreement with the results of the calculations indicating that the experimental data are compatible with several different conformers of the internal loop (Figure 7). The ^{1}H-^{13}C cross peaks intensities broadened by exchange suggest interconversion between these conformers. The exchange broadening observed for residue G_4 also suggest that it could be involved in alternative base pairings with C_{22} and C_{23}.

Stabilities of extended and mutant mini-cTAR DNAs

Although the lower part of the cTAR stem is AT-rich and contains bulged nucleotides (Figure 1), we cannot totally exclude the possibility that the structural and dynamic properties of the mini-cTAR hairpin are due in part to the truncation of the cTAR stem. To test this hypothesis, mini-cTAR was extended by seven residues and the resulting molecule (33 residues long) was called Emini-cTAR (Figure 1). Analysis of the imino to amino region of the NOESY spectra at 10°C allowed the assignment of resonances (Figure 9A). Since the resonances of the residues of the common part of mini-cTAR and Emini-cTAR have nearly identical chemical shifts, it can be deduced that the folding of Emini-cTAR is similar to that of mini-cTAR, i.e. the mini-cTAR and Emini-cTAR molecules form apical and internal loops and upper and lower stems of similar size. The imino protons corresponding to the base pairing interaction between nucleotides $_{-3}TAG_{-1}$ and $_{28}CTA_{30}$ (Figure 1) are not detected (Figure 9A). Fraying of the ends of Emini-cTAR and the loose AT base pairs are probably responsible for the absence of the expected imino protons. Therefore, the base pairing interaction between nucleotides $_{-3}TAG_{-1}$ and $_{28}CTA_{30}$ is weak or does not occur. In addition, analysis of the imino to amino region of the NOESY spectra at 10°C shows the presence of the four imino cross-peaks already observed in mini-cTAR and two additional G imino signals (Figure 9A). The additional signals were assigned on the basis of their connectivities to the H5 resonances previously assigned. These imino protons are those of residues G_{25} and G_{26} and were not detected in mini-cTAR (Figure 3). Thus, the fraying of the C_1-G_{26} and C_2-G_{25} base pairs in mini-cTAR is suppressed in Emini-cTAR, i.e. the C_1-G_{26} and C_2-G_{25} base pairs have been stabilized in the extended mini-cTAR. However, the major point is that the imino protons of the G_4-C_{23} and A_3-T_{24} base pairs adjacent to the internal loop are not observed confirming thus the data obtained with the mini-cTAR molecule. These data suggest large differences in stability between the upper and lower stems of Emini-cTAR. Therefore, these results are consistent with the hypothesis that the internal loop destabilizes the lower stems of mini-cTAR and Emini-cTAR.

To show that the putative destabilizing effect of the internal loop depends on its asymmetry, the Emini-cTARm mutant was designed (Figure 1). In Emini-cTARm, a single-point-mutation (G_6 to C_6) shortens the upper stem and decreases the asymmetry of the internal loop. In the absence of NC, the annealing of mini-cTAR to mini TAR is a slow process that is initiated through a loop–loop interaction (15). The G_6A_6 mutation, designed to shorten and destabilize the upper stem of mini-cTAR, facilitates the annealing of mini-cTAR to mini TAR (15). Similar to mini-cTAR annealing, the annealing of Emini-cTAR to mini-TAR is facilitated by the G_6C_6 mutation (Supplementary Figure 3). The imino region of spectra of Emini-cTARm are characterized by several changes as compared with those of Emini-cTAR (Figure 9): (i) two signals, whose one is very broad (not detected in the 2D spectra), are observed in the 14–14.5 ppm region corresponding to the AT base pairs region; (ii) absence of the G_6 imino proton signal in the 12.8-13 ppm region because the G_6–C_{19} base pair is suppressed by the

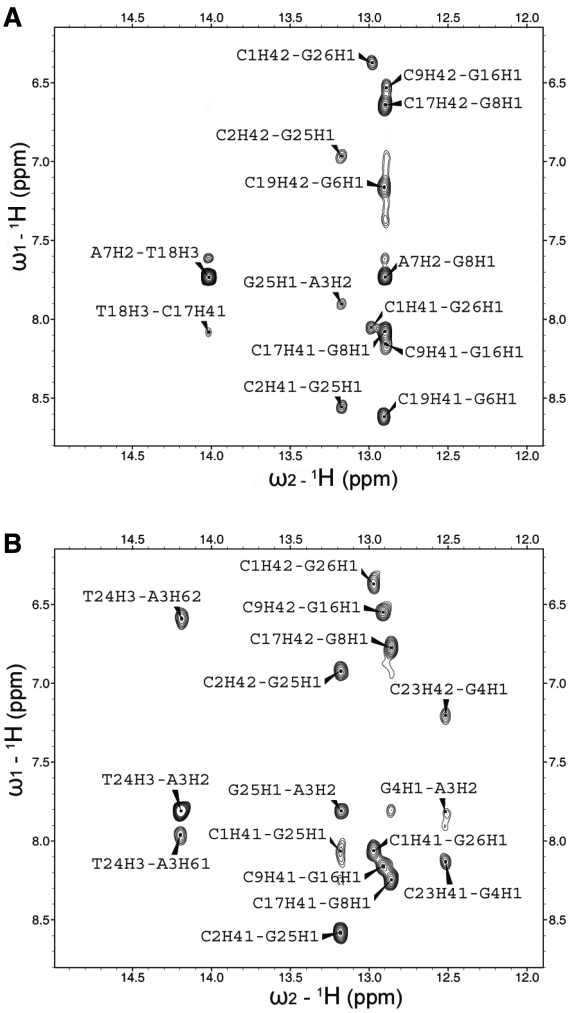

Figure 9. NMR spectra of the extended mini-cTAR DNAs. (**A**) Selected region of 2D NOESY (200 ms) spectrum of Emini-cTAR at 10°C recorded in the same conditions than that presented in Figure 3. The region is that of imino to H2/amino connectivities. The main intra and inter base-pairs cross-peaks are labeled and the involved protons are indicated. Relative to the spectrum of Figure 3, two additional imino protons are observed corresponding to the C_1-G_{26} and C_2-G_{25} base pairs. (**B**) Selected region of 2D NOESY (200 ms) spectrum of Emini-cTARm at 10°C. The region is that of imino to H2/amino connectivities. The main intra and inter base-pairs cross-peaks are labeled and the involved protons are indicated. The appearance of new signals is discussed in the Results section.

single-point-mutation; (iii) appearance of one new G imino proton peak near 12.5 ppm The imino–imino region of the NOESY spectra allows us to assign the new signals (Supplementary Figure 4). The T signal at 14.2 ppm could be assigned to the T_{24} imino proton because it correlates with the G_{25} imino proton resonance near 13.2 ppm that was previously assigned in Emini-cTAR (Figure 9A). The other T signal, broad in the 1D spectra but not detected in the 2D spectra, is thus the T_{18} signal that is strongly affected by the G_6-C_{19} base pair loss in the upper stem of Emini-cTARm. The T_{24} imino proton correlates with the new G imino proton appearing at 12.5 ppm (Supplementary Figure 4) and this corresponds then to the G_4 imino proton. These data indicate that the four imino protons of the lower stem are detected, i.e. the base-pairs forming the lower stem are stable in the extended mutant. Thus, a single-point mutation decreasing the asymmetry of the internal loop may stabilize the lower stem.

Interestingly, ^{1}H–^{13}C HSQC analyses of Emini-cTAR and Emini-cTARm (Supplementary Figure 5) showed that the H1′–C1′ cross peak intensity for the G_4 residue is much higher for the mutant (signal at 5.4 ppm) than for the wild-type (signal at 5.7 ppm). These data strongly suggest that conformational exchange in the lower stem is abolished or strongly reduced in the Emini-cTARm, due to the tight pairing of G_4 and C_{23}.

DISCUSSION

The different parts of mini-cTAR display different stabilities and motions

The mini-TAR RNA structure in the presence and absence of various ligands has been extensively studied by NMR methods (16,17,19,30,32,33). However, its DNA counterpart, the mini-cTAR molecule, has not been the subject of similar studies. NMR investigations showed that the binding of ligands (for example, argininamide and magnesium) to mini-TAR RNA induces the rearrangement of stems that are separated by an internal loop (19,32,34). The ligands arrest the relative motions of the two stems around the internal loop that acts as a hinge (19,32).

Mini-cTAR undergoes various motions occurring in a large range of timescales. The motional properties can be characterized by (i) the fact that for both apical and internal loops the calculations did not show any convergence and demonstrate that NMR data are compatible with several conformers; (ii) analysis of ^{1}H–^{13}C HSQC spectra and particularly the C1′–H1′ regions reveals slow motions in the micro-to millisecond timescale in the internal loop, and faster motions (nano-to picosecond) in the apical loop. These latter data are in agreement with COSY and NOE data. Motions faster than overall tumbling are revealed through anomalously high intensities in HSQC spectra but the H5–H6 COSY cross-peaks are also informative (30). We should, however, make distinctions in the pattern of cross-peaks observed for the various cytosines: (i) the cytosines C_{11}, C_{12}, C_{13} (residues of the apical loop) which have high cross-peaks intensities in both the COSY and HSQC spectra (Figures 4 and 8) and (ii) residues C_2 and C_{23} (in the lower stem) which have high intensities in the COSY cross-peaks but the C1′–H1′ intensities of their HSQC cross-peaks are close to those of the upper stem (Figures 4 and 8). Thus, we can infer that the lower stem is animated by motions slower than those of the apical loop, but faster than those of the upper stem. This is in agreement with the lower stem appearing to be weakly structured and dynamic as suggested by the non observation of its imino protons and the analysis of calculations. In addition, structural probing with single-strand specific nucleases and $KMnO_4$ provides strong evidence that the lower stem is not stable (Figure 2). The apical loop, particularly at the cytosine sites is highly dynamic and did not display any degree of organization. As expected, single-strand specific nucleases cleave the apical loop between residues C_{12}, C_{13} and C_{13}, G_{14} (Figure 2). Residues C_{12} and C_{13} of the apical loop are thus completely accessible for interactions with the TAR apical loop. However, the H1′–C1′ HSQC cross-peak intensities did not show that the other residues of the apical loop, T_{10}, G_{14} and G_{15}, are animated with fast motions (Figure 8). Therefore, these residues are probably more involved than residues C_{12} and C_{13} of the apical loop in interactions with other nucleotides. Indeed, the structure calculations indicate that residue T_{10} exhibits moderate and weak stacking interactions with residues C_9 and C_{11}, respectively.

Our most surprising finding was the small number of observable imino protons in mini-cTAR: there were only four signals (Figure 3) although at least eight Watson–Crick base-pairs were expected from the predicted secondary structure (Figure 1). In agreement with this, Beltz *et al.* (14) reported that the free energy of mini-cTAR is similar to that of hairpins with only four to six base-pairs. These data are confirmed by the experiments conducted on Emini-cTAR showing a number of imino protons smaller than those expected. The two imino signals characterizing the T.G mismatch were not detected in NMR experiments, so the T.G base pair predicted by mfold (Figure 1) was presumably not formed under our conditions. Therefore, the apical loop is constituted of six but not four residues, these being available to pair with the six complementary residues of the apical loop of the cognate TAR hairpin loop. Four base-pairs form the upper stem that is recognized by the double-strand-specific DNase I (Figure 2). There was strong DNAse I cleavage at the junction of the loop and stem: this type of DNase I cleavage has previously been described for DNA hairpins (35).

The non observation of imino protons of the lower stem is in agreement with destabilization of the base pairs of this stem. However, we cannot totally exclude the possibility that the non observation of imino protons could be associated to a particular structure in which the imino protons are exposed to rapid exchange with the solvent. High mobility of residues in the lower stem (COSY data, Figure 4) and the probing experiments (Figure 2) provide additional data supporting the notion that the lower stem is weakly structured and dynamic. We found that the conversion of G_6 to C_6 (mutant Emini-cTARm) provides an apparent stabilization of the lower helix. This mutation

increases the size of the internal loop and makes it less asymmetric [2 (left)/4(right) residues versus 1/3 residues]. One can surmise that this change decreases the degree of backbone distortion at the junction of the loop and lower stem. Interestingly, an early study using oligoribonucleotides showed that asymmetric loops destabilize a helix more than symmetric loops (36). Vo *et al.* (15) studied the conversion of G_6 to A_6 that decreases the asymmetry of the internal loop and probably stabilizes the lower stem. The G_6A_6 mutation increases the annealing of mini-cTAR DNA to mini-TAR RNA. This observation is probably due to shortening of the upper stem that is therefore less stable in the mutant than in the wild-type. Similarly, the G_6C_6 mutation facilitates the annealing of Emini-cTARm DNA to mini-TAR RNA (Supplementary Figure 3). These results support the notion that the apical loops are the initiation sites for the annealing reaction in the absence of NC (6,15).

Conformational exchange in the internal loop affects the lower stem stability

The internal loop is probably responsible for the destabilization of the base pairs of the lower stem and it was shown that its deletion increases the stability of mini-cTAR (14). Our study allows a better understanding of the mechanism of this destabilization by the internal loop (see below). The extended mini-cTAR DNA (Emini-cTAR) allows us to discriminate between the destabilizing effects of the internal loop and end-fraying. We showed that the lower stem becomes stable when the length of the internal loop of Emini-cTAR is increased by a single-point mutation (Figure 9). Our data obtained with mini-cTAR and the extended constructs demonstrate that the internal loop is responsible for asymmetric destabilization of the top half of the cTAR DNA hairpin. Residues A_5, G_{20} and A_{21} in the internal loop display conformational exchange, and these features extend to the neighboring residues (Figure 8B). Note that residue G_4 is more affected than the residues of the upper stem. The exchange-broadened residues probably sample several conformations. Analysis of the best-energy conformers calculated from NMR data indicates that residue A_5 could pair with residues G_{20} and A_{21} (Figure 7) and residue G_4 with residue C_{23}. The equally possible pairing of residue G_4 with residue C_{22} suggests that residue G_4 has an alternative pairing. This possibility was previously suggested by Beltz *et al.* (14). The slow motions in the internal loop are probably related to alternative possibilities of base pairing involving the residues of the loop and those adjacent to the lower stem. The propagation of these slow motions in the lower stem could be linked to the destabilization of the molecule. Our data, and particularly the highly low-field-shifted phosphorus signal (Figure 5), also show that the G_4pA_5 segment connecting the internal loop to the lower stem is strongly distorted. In contrast, the A_5pG_6 connecting the internal loop to the upper stem is not distorted. These features underline the asymmetric influence of the internal loop on the neighboring stems. Here, the distorted backbone is associated with the lower stem destabilization. Finally, our data are of general interest to the understanding of how an internal loop destabilizes a DNA stem. Interestingly, it has been reported that an internal loop could asymmetrically destabilize the adjacent stems: asymmetric destabilization has been described for the SL1 stem-loop involved in the dimerization of the HIV-1 genomic RNA (31,37) and for the HIV-1 frameshifting RNA signal (38).

Role of the dynamics of the top half of cTAR in its functional properties

Mini-cTAR represents the top half of cTAR that is involved in the TAR RNA/DNA annealing process. The particular dynamic properties of the top half of cTAR may make a substantial contribution to its functional properties, i.e. in promoting the transition towards the extended duplex and in its destabilization by NC. The flexibility introduced by the internal loop could promote the 'kissing' complex to extended dimer transition. An attractive possibility is that the loop–loop interaction brings the internal loops of TAR and cTAR into close proximity such that they can then pair. Indeed, two cytosines of cTAR (numbered C_{22} and C_{23} in mini-cTAR) are weakly paired, due to conformational exchange, and could pair with residues G_{20} and G_{21} of TAR that are adjacent to the internal bulge (Figure 1). Probing data show these latter residues to be relatively exposed (6). Such interactions could provide a second point of contact between cTAR and TAR that would favor the transition towards the extended duplex. NMR analysis indicates that mini-TAR is highly stable and that the two stems are fully paired (30,39); it does not provide evidence for significant exchange broadening in and around the bulge (30,39). Motions in the range of the nanosecond-to-microsecond and not in the range of microsecond to millisecond have been observed in two studies (39,40). In contrast, mini-cTAR is highly destabilized and the lower stem does not display a stable pairing. The internal loop residues show significant exchanges broadening that are compatible with motions in the microsecond-to-millisecond range. The existence of these motions seems to have a profound impact on the stability of mini-cTAR. The intrinsically low stability of cTAR may make its destabilization by NC easier than that of TAR which is highly structured. Indeed, NC has a greater effect on the destabilization of cTAR DNA than on TAR RNA (41).

Finally, our data show that the upper part of the cTAR DNA hairpin undergoes various motions and lead to novel explanations of the role of the top half of cTAR in the annealing process. It would be useful to determine whether these motions change when the cTAR molecule interacts with various partners, particularly the TAR molecule, magnesium and NC. Moreover, NC probably interacts with the internal loop of cTAR (14). In conclusion, our study shows that a DNA sequence, in a manner similar to that of an RNA sequence, encodes a complex pattern of motions related to its various functions.

SUPPLEMENTARY DATA

Supplementary Data are available at NAR Online.

FUNDING

Agence Nationale de Recherches sur le Sida (to P.F. and O.M.). Postdoctoral fellowship from Agence Nationale de Recherches sur le Sida (to I.K.). Funding for open access charge: CNRS.

Conflict of interest statement. None declared.

REFERENCES

1. Katz,R.A. and Skalka,A.M. (1994) The retroviral enzymes. *Annu. Rev. Biochem.*, **63**, 133–173.
2. Levin,J.G., Guo,J., Rouzina,I. and Musier-Forsyth,K. (2005) Nucleic acid chaperone activity of HIV-1 nucleocapsid protein: critical role in reverse transcription and molecular mechanism. *Prog. Nucleic Acid Res. Mol. Biol.*, **80**, 217–286.
3. Berkhout,B., Klaver,B. and Das,A.T. (1995) A conserved hairpin structure predicted for the poly(A) signal of human and simian immunodeficiency viruses. *Virology*, **207**, 276–281.
4. Darlix,J.L., Vincent,A., Gabus,C., de,R.H. and Roques,B. (1993) Trans-activation of the 5′ to 3′ viral DNA strand transfer by nucleocapsid protein during reverse transcription of HIV1 RNA. *C. R. Acad. Sci. III*, **316**, 763–771.
5. Berkhout,B., Vastenhouw,N.L., Klasens,B.I. and Huthoff,H. (2001) Structural features in the HIV-1 repeat region facilitate strand transfer during reverse transcription. *RNA*, **7**, 1097–1114.
6. Kanevsky,I., Chaminade,F., Ficheux,D., Moumen,A., Gorelick,R., Negroni,M., Darlix,J.L. and Fosse,P. (2005) Specific interactions between HIV-1 nucleocapsid protein and the TAR element. *J. Mol. Biol.*, **348**, 1059–1077.
7. Moumen,A., Polomack,L., Roques,B., Buc,H. and Negroni,M. (2001) The HIV-1 repeated sequence R as a robust hot-spot for copy-choice recombination. *Nucleic Acids Res.*, **29**, 3814–3821.
8. You,J.C. and McHenry,C.S. (1994) Human immunodeficiency virus nucleocapsid protein accelerates strand transfer of the terminally redundant sequences involved in reverse transcription. *J. Biol. Chem.*, **269**, 31491–31495.
9. Godet,J., de Rocquigny,H., Raja,C., Glasser,N., Ficheux,D., Darlix,J.L. and Mely,Y. (2006) During the early phase of HIV-1 DNA synthesis, nucleocapsid protein directs hybridization of the TAR complementary sequences via the ends of their double-stranded stem. *J. Mol. Biol.*, **356**, 1180–1192.
10. Liu,H.W., Cosa,G., Landes,C.F., Zeng,Y., Kovaleski,B.J., Mullen,D.G., Barany,G., Musier-Forsyth,K. and Barbara,P.F. (2005) Single-molecule FRET studies of important intermediates in the nucleocapsid-protein-chaperoned minus-strand transfer step in HIV-1 reverse transcription. *Biophys. J.*, **89**, 3470–3479.
11. Liu,H.W., Zeng,Y., Landes,C.F., Kim,Y.J., Zhu,Y., Ma,X., Vo,M.N., Musier-Forsyth,K. and Barbara,P.F. (2007) Insights on the role of nucleic acid/protein interactions in chaperoned nucleic acid rearrangements of HIV-1 reverse transcription. *Proc. Natl Acad. Sci. USA*, **104**, 5261–5267.
12. Zeng,Y., Liu,H.W., Landes,C.F., Kim,Y.J., Ma,X., Zhu,Y., Musier-Forsyth,K. and Barbara,P.F. (2007) Probing nucleation, reverse annealing, and chaperone function along the reaction path of HIV-1 single-strand transfer. *Proc. Natl Acad. Sci. USA*, **104**, 12651–12656.
13. Beltz,H., Azoulay,J., Bernacchi,S., Clamme,J.P., Ficheux,D., Roques,B., Darlix,J.L. and Mely,Y. (2003) Impact of the terminal bulges of HIV-1 cTAR DNA on its stability and the destabilizing activity of the nucleocapsid protein NCp7. *J. Mol. Biol.*, **328**, 95–108.
14. Beltz,H., Piemont,E., Schaub,E., Ficheux,D., Roques,B., Darlix,J.L. and Mely,Y. (2004) Role of the structure of the top half of HIV-1 cTAR DNA on the nucleic acid destabilizing activity of the nucleocapsid protein NCp7. *J. Mol. Biol.*, **338**, 711–723.
15. Vo,M.N., Barany,G., Rouzina,I. and Musier-Forsyth,K. (2006) Mechanistic studies of mini-TAR RNA/DNA annealing in the absence and presence of HIV-1 nucleocapsid protein. *J. Mol. Biol.*, **363**, 244–261.
16. Aboul-ela,F., Karn,J. and Varani,G. (1995) The structure of the human immunodeficiency virus type-1 TAR RNA reveals principles of RNA recognition by Tat protein. *J. Mol. Biol.*, **253**, 313–332.
17. Puglisi,J.D., Tan,R., Calnan,B.J., Frankel,A.D. and Williamson,J.R. (1992) Conformation of the TAR RNA-arginine complex by NMR spectroscopy. *Science*, **257**, 76–80.
18. Jaeger,J.A. and Tinoco,I. Jr. (1993) An NMR study of the HIV-1 TAR element hairpin. *Biochemistry*, **32**, 12522–12530.
19. Al Hashimi,H.M., Gosser,Y., Gorin,A., Hu,W., Majumdar,A. and Patel,D.J. (2002) Concerted motions in HIV-1 TAR RNA may allow access to bound state conformations: RNA dynamics from NMR residual dipolar couplings. *J. Mol. Biol.*, **315**, 95–102.
20. Hirao,I., Kawai,G., Yoshizawa,S., Nishimura,Y., Ishido,Y., Watanabe,K. and Miura,K. (1994) Most compact hairpin-turn structure exerted by a short DNA fragment, d(GCGAAGC) in solution: an extraordinarily stable structure resistant to nucleases and heat. *Nucleic Acids Res.*, **22**, 576–582.
21. Maxam,A.M. and Gilbert,W. (1980) Sequencing end-labeled DNA with base-specific chemical cleavages. *Methods Enzymol.*, **65**, 499–560.
22. Renisio,J.G., Cosquer,S., Cherrak,I., El Antri,S., Mauffret,O. and Fermandjian,S. (2005) Pre-organized structure of viral DNA at the binding-processing site of HIV-1 integrase. *Nucleic Acids Res.*, **33**, 1970–1981.
23. Stallings,S.C. and Moore,P.B. (1997) The structure of an essential splicing element: stem loop IIa from yeast U2 snRNA. *Structure*, **5**, 1173–1185.
24. Schwieters,C.D., Kuszewski,J.J., Tjandra,N. and Clore,G.M. (2003) The Xplor-NIH NMR molecular structure determination package. *J. Magn Reson.*, **160**, 65–73.
25. Desai,N.A. and Shankar,V. (2003) Single-strand-specific nucleases. *FEMS Microbiol. Rev.*, **26**, 457–491.
26. Hampshire,A.J., Rusling,D.A., Broughton-Head,V.J. and Fox,K.R. (2007) Footprinting: a method for determining the sequence selectivity, affinity and kinetics of DNA-binding ligands. *Methods*, **42**, 128–140.
27. Holstege,F.C. and Timmers,H.T. (1997) Analysis of open complex formation during RNA polymerase II transcription initiation using heteroduplex templates and potassium permanganate probing. *Methods*, **12**, 203–211.
28. Craig,M.L., Tsodikov,O.V., McQuade,K.L., Schlax,P.E. Jr, Capp,M.W., Saecker,R.M. and Record,M.T. Jr. (1998) DNA footprints of the two kinetically significant intermediates in formation of an RNA polymerase-promoter open complex: evidence that interactions with start site and downstream DNA induce sequential conformational changes in polymerase and DNA. *J. Mol. Biol.*, **283**, 741–756.
29. Rubin,C.M. and Schmid,C.W. (1980) Pyrimidine-specific chemical reactions useful for DNA sequencing. *Nucleic Acids Res.*, **8**, 4613–4619.
30. Zhang,Q., Sun,X., Watt,E.D. and Al Hashimi,H.M. (2006) Resolving the motional modes that code for RNA adaptation. *Science*, **311**, 653–656.
31. Sun,X., Zhang,Q. and Al Hashimi,H.M. (2007) Resolving fast and slow motions in the internal loop containing stem-loop 1 of HIV-1 that are modulated by Mg2+ binding: role in the kissing-duplex structural transition. *Nucleic Acids Res.*, **35**, 1698–1713.
32. Pitt,S.W., Majumdar,A., Serganov,A., Patel,D.J. and Al Hashimi,H.M. (2004) Argininamide binding arrests global motions in HIV-1 TAR RNA: comparison with Mg2+-induced conformational stabilization. *J. Mol. Biol.*, **338**, 7–16.
33. Chang,K.Y. and Tinoco,I. Jr. (1997) The structure of an RNA 'kissing' hairpin complex of the HIV TAR hairpin loop and its complement. *J. Mol. Biol.*, **269**, 52–66.
34. Al Hashimi,H.M., Pitt,S.W., Majumdar,A., Xu,W. and Patel,D.J. (2003) Mg2+-induced variations in the conformation and dynamics of HIV-1 TAR RNA probed using NMR residual dipolar couplings. *J. Mol. Biol.*, **329**, 867–873.
35. Potaman,V.N., Shlyakhtenko,L.S., Oussatcheva,E.A., Lyubchenko,Y.L. and Soldatenkov,V.A. (2005) Specific binding of poly(ADP-ribose) polymerase-1 to cruciform hairpins. *J. Mol. Biol.*, **348**, 609–615.
36. Peritz,A.E., Kierzek,R., Sugimoto,N. and Turner,D.H. (1991) Thermodynamic study of internal loops in oligoribonucleotides:

symmetric loops are more stable than asymmetric loops. *Biochemistry*, **30**, 6428–6436.
37. Mazier,S. and Genest,D. (2007) Molecular dynamics simulation for probing the flexibility of the 35 nucleotide SL1 sequence kissing complex from HIV-1Lai genomic RNA. *J. Biomol. Struct. Dyn.*, **24**, 471–479.
38. Gaudin,C., Mazauric,M.H., Traikia,M., Guittet,E., Yoshizawa,S. and Fourmy,D. (2005) Structure of the RNA signal essential for translational frameshifting in HIV-1. *J. Mol. Biol.*, **349**, 1024–1035.
39. Zhang,Q., Stelzer,A.C., Fisher,C.K. and Al Hashimi,H.M. (2007) Visualizing spatially correlated dynamics that directs RNA conformational transitions. *Nature*, **450**, 1263–1267.
40. Olsen,G.L., Echodu,D.C., Shajani,Z., Bardaro,M.F., ,Jr., Varani,G. and Drobny,G.P. (2008) Solid-state deuterium NMR studies reveal micros-ns motions in the HIV-1 transactivation response RNA recognition site. *J. Am. Chem. Soc.*, **130**, 2896–2897.
41. Bernacchi,S., Stoylov,S., Piemont,E., Ficheux,D., Roques,B.P., Darlix,J.L. and Mely,Y. (2002) HIV-1 nucleocapsid protein activates transient melting of least stable parts of the secondary structure of TAR and its complementary sequence. *J. Mol. Biol.*, **317**, 385–399.
42. Zuker,M. (2003) Mfold web server for nucleic acid folding and hybridization prediction. *Nucleic Acids Res.*, **31**, 3406–3415.